Applied Physics B (2020) 126:192
https://doi.org/10.1007/s00340-020-07544-y

Applied Physics B
Lasers and Optics

Growth and characterization of InP-based 1750 nm emitting membrane external-cavity surface-emitting laser

Artur Broda[1] · Bartosz Jeżewski[1] · Iwona Sankowska[1] · Michał Szymański[2] · Paweł Hoser[2] · Jan Muszalski[1]

Received: 26 December 2019 / Accepted: 18 October 2020 / Published online: 3 November 2020

Abstract
The epitaxial growth and emission properties of a membrane external-cavity surface-emitting laser (MECSEL) are demonstrated in the 1750 nm band. A heterostructure consisting of InGaAs quantum wells enclosed by InGaAlAs barriers was deposited on InP by molecular beam epitaxy. The emitted power exceeded 1.5 W, which is the highest that has been reported in this spectral range to date.

1 Introduction

It has been proven over the last 2 decades that semiconductor heterostructures can be used as a valuable gain medium in external resonator lasers [1]. The simplicity of fabricating discs from epitaxial material leads to a demonstration of optically pumped vertical cavity surface-emitting semiconductor lasers (VECSEL), emitting at wavelengths ranging from red to infrared [2, 3]. The conventional VECSEL consists of a semiconductor active mirror and one or more external dielectric mirrors constituting the resonator. The active mirror is appropriately mounted on a heatsink semiconductor heterostructure consisting of monolithically integrated active region quantum wells (QW) or quantum dots (QD) and distributed Bragg reflectors (DBRs). The wavelength flexibility due to the bandgap engineering of epitaxially grown semiconductor heterostructures is the unique feature of VECSELs. The emission in 920–1180 nm range has been demonstrated using single material set technology consisting of strain-compensated InGaAs/GaAsP quantum wells (QW) grown on GaAs substrates [4, 5]. Output power exceeding 100 W at 1048 nm has been demonstrated with this technology [6]. This is the highest power ever emitted by a single emitter of any semiconductor laser. The spectrally broad gain of QW permitted for broad tuning from 21 and 156 nm at 665 nm and 1970 nm wavelength, respectively, using intra-cavity birefringent. For emission in the 1750 nm band, tuning as broad as 120 nm could be expected [7]. The short lifetime of spontaneous emission in semiconductor materials in certain applications is also an advantage. It makes VECSEL class A lasers free of relaxation oscillation. Compared to most solid-state lasers, the VECSELs have minor requirements for the optical pump's wavelength: the photon energy has to be larger than the absorber bandgap. Due to the semiconductor's spectrally broad and high absorption, stabilization of the pump's wavelength or beam recycling are not needed. The VECSEL external resonator assures the high optical beam quality. The external dielectric mirrors enable the discrimination of the higher order modes. A single lateral mode emission with a power of 20 W has been demonstrated [8]. A single-frequency VECSEL with an intra-cavity birefringent filter and etalon emitting 23 W have also been demonstrated [9]. A spectral linewidth of only 75 kHz was shown for a VECSEL [10].

In spite of those advantages, the spectral range above the telecommunication band of 1550 nm and below 2000 nm is very weakly penetrated by optically pumped surface-emitting semiconductor lasers [2, 3]. This is due to the low quality of epitaxially grown DBRs determined by the low index contrast of compounds lattice matched to InP [11]. In shorter wave infrared spectral regions, the success of the surface emitters comes from DBRs composed of GaAs and AlGaAs layers. The low lattice mismatch between GaAs and AlAs enables the growth of thick pseudomorphic multilayer stacks with large numbers of quarter-wavelength layer pairs, which

✉ Jan Muszalski
jan.muszalski@imif.lukasiewicz.gov.pl

[1] Łukasiewicz Research Network, Institute of Microelectronics and Photonics, Al. Lotników 32/46, 02-668 Warsaw, Poland

[2] Institute of Information Technology, Warsaw University of Life Sciences, SGGW, 159, 02-776 Warsaw, Nowoursynowska, Poland

together with a relatively high refraction index contrast of 0.5 provides a reflectivity close to unity. The drawback is that a GaAs substrate is not suitable for the growth of QWs or QD that are capable of efficient emission in the 1550–1900 nm range. It has been demonstrated that InGaAsNSb QWs lattice-matched to GaAs, despite providing gain, are not suitable for high-power emission [12]. The GaSb lattice-matched heterostructures are not competitive in this spectral range. The refraction index contrast between the GaAlAsSb and AlAsSb layers can reach 0.4, thus providing high DBR reflectivity, but these materials have a bandgap that is too narrow. The shortest wavelength emission of a GaSb lattice-matched laser that has been demonstrated so far is 1920 nm [13].

The only suitable quantum wells for emission in the 1550–1900 spectral region are strained InGaAs QWs lattice-matched to InP. However, the growth of highly reflective DBRs on InP substrate is not possible, due to the low index contrast between the InP-matched InAlAs and the InGaInAs or InGaAsP compounds [11]. Even more than 30 pairs of the quarter-wavelength layers do not improve the reflectivity of the DBRs. The low refractive index contrast implies that the optical wave penetrates greater depths, and therefore, there is larger absorption due to the free carriers and scattering losses due to the limited crystal quality of the interfaces [14, 15]. There are two solutions for this contradiction: the growth of DBRs on GaAs and wafer bonding/fusion with the active region grown on InP, or growth of just the active region without DBRs. The first solution enables the fabrication of electrically driven vertical-cavity surface-emitting-lasers (VCSELs) [11] or optically pumped vertical-external-cavity surface-emitting lasers (VECSELs) [16–18]. The structure without DBRs constitutes the gain element of the DBR-free laser, also called an MECSEL [19, 20]. MECSELs and VECSELs both offer laser beams with high-power and high optical quality, but MECSELs offer a higher wavelength flexibility when compared with VECSELs [20, 21].

Using the InP-based MECSEL technology permits the advantages of optically pumped semiconductor lasers to be explored in the 1550–1900 nm spectral range as well. Many applications need a high-power, beam with good optical quality and low-cost laser sources in this spectral region. The optical pumping of Cr+2:ZnSe lasers and the processing of plastics or solids that contain water are some of the most obvious applications, of many.

Here, we report for the first time the successful growth of heterostructures of a MECSEL lattice-matched to InP, and the high-power emission of a MECSEL in the 1750 nm spectral range. Neither a VCSEL, VECSEL nor a MECSEL has yet been demonstrated in this spectral region.

2 Heterostructure design and growth

For emission in the 1750 nm band, the InGaAs QWs enclosed by thick InGaAlAs barriers were designed using the PICS3D commercial software by Crosslight [22]. The wavelength emission of the QWs is set based on the QW's thickness and the composition of the QWs and the barriers which can affect the discontinuity of conduction and valence band potential. The main constraint in the case of the lattice mismatch is, however, the critical thickness for the pseudomorphic growth of the QWs. A thickness of 8 nm is commonly used in semiconductor technology because of the high carrier capture cross-section [23]. This value was also chosen for our MECSEL. This determined the high indium content of $x = 0.7$ in the $In_xGa_{1-x}As$ QW, introducing the high strain of $\varepsilon = 1.2\%$. For this QW composition, the critical thickness calculated according to Matthews et al. [24] is 19 nm. A thinner QW would require a higher content of In, which in turn would result in an even higher strain and a lower critical thickness. Thus, it would be impossible to epitaxially grow a heterostructure on an InP substrate without the deterioration of crystalline perfection.

The barriers' design is more flexible since they are composed of an InGaAlAs alloy containing three metal specimens. However, there are many requirements for the barriers' composition, which determines the laser properties. The barriers should provide QW stress compensation, efficient carrier confinement in the QW, high absorption of pump radiation, and must be feasible based on the chosen technique for epitaxial growth.

For QW stress compensation, barriers composed of $In_{0.52}(Ga_{1-x}Al_x)_{0.48}As$ are required. The lower amount of In in comparison with lattice-matched $In_{0.53}(Ga_{1-x}Al_x)_{0.47}As$ is sufficient, as the barriers' thickness is much larger than the thickness of the QW. The large difference in the thickness of the QWs and the barrier layer does not allow for strain compensation engineering, as it does in the short period superlattices applied in quantum cascade lasers. Here in the MECSELs, the strain is concentrated almost exclusively in the QWs.

For efficient carrier confinement, the discontinuity of the bandgap should be as large as possible. This can be done in $In_{0.53}(Ga_{1-x}Al_x)_{0.47}As$ without changing the lattice constant by providing a high aluminium content. However, too high a barrier energy in the conduction band gives rise to a second quantum level in a QW. This is a disadvantage for any laser, since the carriers fill the higher energy states and do not participate to gain; they may thus give rise to larger spontaneous emission losses. Conversely, low bandgap barriers in a QW prevent the existence of higher quantum levels. In addition, they allow

for the faster carrier thermalization onto QW levels, as lower energy loss is required. In optically pumped devices where a resonant periodic gain (RPG) schema is employed, the barriers' low bandgap energy permits the use of low photon energy pumping sources. This is favourable since the optical pumping trades one high-energy photon for one of a lower energy. The difference in absorbed and emitted photon energy, the so-called quantum defect, is converted into heat. The benefit of low bandgap barriers when used in an optically pumped VECSEL was proven in the case of a GaSb-based device emitting at 1920 nm [13]. This wavelength is the shortest that has been demonstrated with GaSb-based technology. In this case, the low-energy bandgap of the barriers allowed the use of a 1470 nm pump instead of an equally available 980 nm pump. The use of this low quantum defect pump doubled the power of the emitted light.

In the case of an emitter designed for the emission at a wavelength of 1750 nm, the use of a 1470 nm pump would require the total energy of conduction and valence bands barriers to be smaller than 135 meV. This small value would not provide sufficient confinement for carriers, especially electrons, which would result in carrier leakage. If elevated active region temperatures are present during the laser operation, the thermally activated carriers could escape to the waveguide, where they would recombine through a radiative or nonradiative channel. This process would decrease the T_0 parameter [25]. It is expected that the low thermal conductivity and large thickness of a quaternary $In_{0.52}(Ga_{0.5}Al_{0.5})_{0.48}As$ alloy (6 W/mK) will substantially increase the temperature in the active region, and thus high energy bandgap barriers are necessary. Consequently, the heterostructure was designed to be pumped using 980 nm radiation, provided by widely available and cost-effective high-power semiconductor laser pumps. A numerical simulation has shown that at elevated temperature for a QW barrier with a larger bandgap, there is a higher gain at any given carrier concentration. Therefore, a barrier composition of $In_{0.52}(Ga_{0.5}Al_{0.5})_{0.48.}$ As was selected, with a bandgap energy equal to 1.1 eV [26]. The conduction band, heavy hole's valence band, and light hole's valence band offsets are 0.360 eV, 0.141 eV, and 0.066 eV, respectively. Consequently, in conduction band of designed QW two quantum levels exist ground 1e and excited 2e level. The calculated gain and reduced density of states are shown in Fig. 1. The energy differences for permitted optical transitions 1e1hh and 1e1lh or 2e2hh are large, being 0.100 eV and over 0.200 eV, respectively.

In this research, molecular beam epitaxy (MBE) was used for the wafer fabrication. In MBE, whenever lattice matching conditions are required, the effusion cells have to be kept at a constant temperature during the growth. Otherwise, it would take minutes to stabilize the flux. Such a long growth

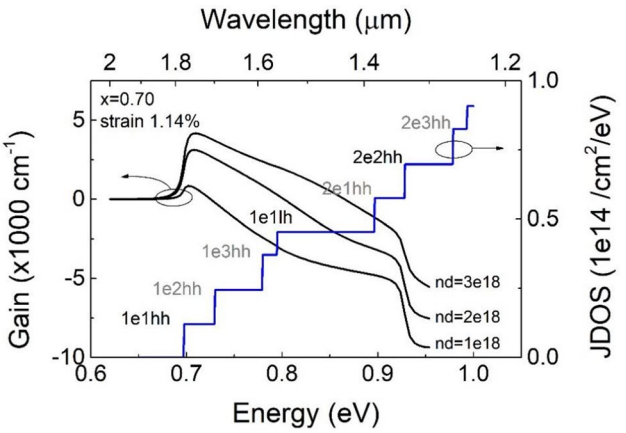

Fig. 1 Calculated gain at 300 K (left scale, black line) and the joint density of states (right scale, blue line) for an 8 nm $In_{0.7}Ga_{0.3}As$ QW enclosed by $In_{0.53}(Ga_{0.5}Al_{0.5})_{0.47}As$ barriers. The calculation was done for a carrier concentration of $n{\cdot}d = 1, 2, 3, \times 10^{18}$ cm^{-3}, where d is the QW thickness

interruption always leads to the substantial deterioration of the epitaxial material. In particular, the radiative recombination deteriorates due to the increased defect concentration. In MBE, instant composition changes can only be realized by instant changes of the shutters' positions of the appropriated cells. In our MBE system, using doubled In and Ga cells and a single Al cell, the layers of $In_{0.52}Al_{0.48}As$ and $In_{0.53}Ga_{0.47}As$ could be grown independently with very similar growth rates, approximately 0.1361 nm/s. The $In_{0.52}(Ga_{0.5}Al_{0.5})_{0.48}As$ composition was realized by combining the aforementioned ternary compounds. Its growth rate was 0.2716 nm/s. The $In_{0.7}Ga_{0.3}As$ QW was grown as $In_{0.52}(Ga_{0.5}Al_{0.5})_{0.48}As$, but with the Al shutter closed. The $In_{0.7}Ga_{0.3}As$ QW growth rate was 0.2064 nm/s.

The MBE growth was carried out in a RIBER Compact 21 T system equipped with standard Knudsen cells for group III elements and a valved cracker cell for arsenic. The growth was carried out on sulphur-doped InP wafers of low etch pit density (EPD) (500 cm^{-1}).

The final MECSEL heterostructure consisted of eight high-indium-content $In_{0.7}Ga_{0.3}As$ QWs, separated by $In_{0.52}(Ga_{0.5}Al_{0.5})_{0.48}As$ barriers (Fig. 2). The QWs and the barriers were 8 nm and 240 nm (λ/2n) thick, respectively. The barrier thicknesses were set to fulfil the RPG schema required for efficient optical pumping and the efficient coupling of gain and the stimulated emission. A 15 nm-thick layer of InGaAs followed by an InAlAs layer was deposited directly on the InP substrate. The same layers but in the reverse order were also deposited on the top of the QW/barrier superlattice (Table 1). The total optical thickness of the MECSEL heterostructure was 11 λ/2. The InAlAs layer was grown to prevent the recombination of photo-carriers via surface states and the InGaAs was grown to protect the

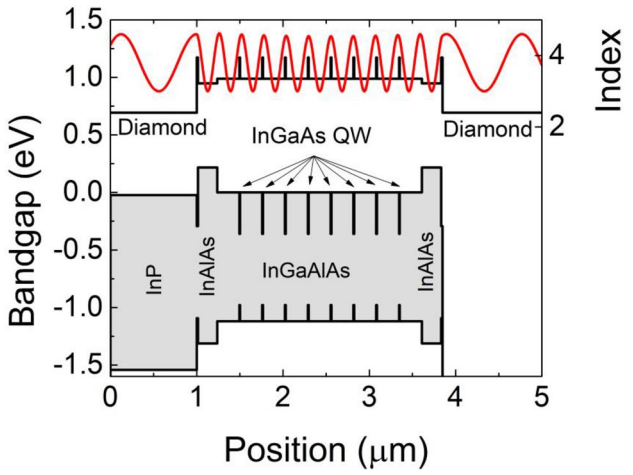

Fig. 2 The bandgap distribution along the growth axis of the As-grown MECSEL wafer grown on InP substrate (bottom, left scale). The refractive index distribution along the same direction of the heterostructure after processing, with removed substrate and bonded in-between two diamonds (top, right scale). The electromagnetic field of longitudinal mode is also shown (top, arbitral units)

Table 1 The MECSEL heterostructure

Function	Composition	Plan D [nm]
Cap	$In_{0.53}Ga_{0.47}As$	15
Window	$In_{0.52}Al_{0.48}As$	223.7
×8	$In_{0.53}(Ga_{0.5}Al_{0.5})_{0.47}As$ Barrier	256.2
	$In_{0.7}Ga_{0.3}As$ QW	8
	$In_{0.53}(Ga_{0.5}Al_{0.5})_{0.47}As$ Barrier	256.2
Window	$In_{0.52}Al_{0.48}As$	223.7
Cap	$In_{0.53}Ga_{0.47}As$	15
Substrate	InP n+	450 λm

InAlAs layer against oxidation. The total thickness of the InAlAs and InGaAs layers was 1λ. On the substrate side, the InGaAs layer was also used as the etch-stop layer. The etch-stop was required to precisely remove the substrate during the post growth processing. In MECSEL technology, the substrate is totally removed for efficient heat extraction. The epitaxial structure is bonded to a single or in-between two transparent heat sinks. Single crystal diamonds are most frequently used as heat sinks due to their high thermal conductivity [27]]. The more cost-effective SiC is also widely used, since single samples of large, good optical quality crystal are available [28, 29]. In this study, after post-growth processing, the laser gain element consisted of a symmetric heterostructure in between two diamond plates enclosed by a copper submount (Fig. 3a). The submount temperature was stabilized by a Peltier element. The gain element was inserted into a symmetric resonator (Fig. 3b). The linear

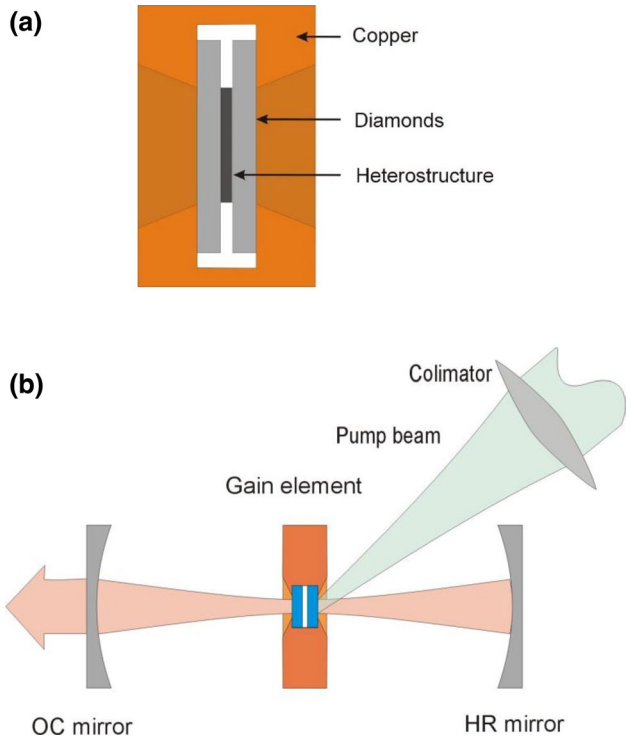

Fig. 3 Schema of the MECSEL gain element (**a**) and the resonator employed for lasing excitation (**b**)

resonator was 200 mm long. It was enclosed by two concave mirrors with radius of curvature equal to 100 mm. The mirrors were coated with high ($R = 0.998$) and partial ($R = 0.985$) reflectivity coatings, respectively. The pump source was a 980 nm semiconductor laser coupled to a fibre. The fibre modal diameter was 200 μm.

The optimum MBE growth parameters were identified prior to the growth of the MECSEL structure. For this task, the special calibration heterostructures were grown and tested using standard room temperature photoluminescence. To simultaneously test the optical properties of many different layers, those expected to emit low-energy photons were grown first, followed by those emitting high energy photons. The buffers of 250 nm thick lattice matched InGaAs were deposited directly on low etch pit density $n+$InP substrates. The structures, which consisted of two single 8 nm thick $In_xGa_{1-x}As$ QWs of low and high indium content, were subsequently enclosed by 50 nm thick quaternary $In_{0.52}(Ga_{0.5}Al_{0.5})_{0.48}As$ barriers. The low indium content $In_xGa_{1-x}As$ QW (nominally $x = 0.53$) was deposited to test the growth conditions of lattice-matched InGaAs QW on a quaternary InGaAlAs barrier layer. The high indium content $In_xGa_{1-x}As$ QW (nominally $x = 0.7$) was grown to test the emission efficiency of the highly strained QW required for emission at 1750 nm. To allow the simultaneous PL characterization of both types of QWs and quaternary 50 nm

thick $In_{0.52}(Ga_{0.5}Al_{0.5})_{0.48}As$ layer, $In_{0.52}Al_{0.48}As$ separation layers were introduced. These wide bandgap 10 nm thick $In_{0.52}Al_{0.48}As$ layers prevented photo-carrier diffusion towards the layers with the lowest bandgap (Fig. 4a).

The test structures were grown under different growth conditions. The As_2 fluxes ($1.1–1.8\times10^{-5}$ Torr) and substrate temperatures (490–520 °C) were changed in-between the heterostructure runs (Fig. 4b). The growth rate was kept constant and equal for particular layers as mentioned above. The growth condition search was limited to the described intervals using previous observations of rapid optical parameter deteriorations caused by InGaAs grown at low temperatures (< 490 °C) or indium desorption at temperatures above 520 °C. The reflection high-energy electron diffraction (RHEED) image indicated a blurred 2×4 reconstruction during the growth of all the heterostructures. The As_2 flux was measured in front of the substrate with a Bayard-Alpert gauge just prior to growth. The substrate temperature was calibrated during the growth of the InGaAs buffer layer using the optical pyrometer. The temperature was not corrected during the heterostructure growth. It has previously been shown that the fluctuation in pyrometer readouts originates from the interferences of thermal radiation reflected at interfaces between the layers of different compositions and the semiconductor-vacuum interface [30].

The PL measurements were performed in a standard setup. A laser emitting at 980 nm was used for excitation. The excitation power was kept at a low value to avoid any heating of the sample. Special attention was paid to all the experimental conditions to ensure they were the same for all the samples so the PL signal intensity could be compared.

3 Wafer characterization and lasing

The photoluminescence data taken at room temperature for the test structures are shown in Fig. 5. The spectra revealed peaks at 1082 nm, 1544 nm, 1637 nm, and 1722 nm which are related to the bandgap transition in $In_{0.53}(Ga_{0.5}Al_{0.5})_{0.48}As$ barriers, InGaAs QW of low indium content, $In_{0.53}Ga_{0.47}As$ buffer, and InGaAs QW of high indium content, respectively. The PL experiment shows that the optimum growth conditions are different for different layers. The highest PL signal for the highly strained $In_{0.7}Ga_{0.3}As$ QW was registered when the sample was grown at a high temperature and with a low As_2 flux. In contrast, the PL intensity of lattice-matched $In_{0.53}Ga_{0.47}As$ QW weakly depended on the growth conditions. It was identical

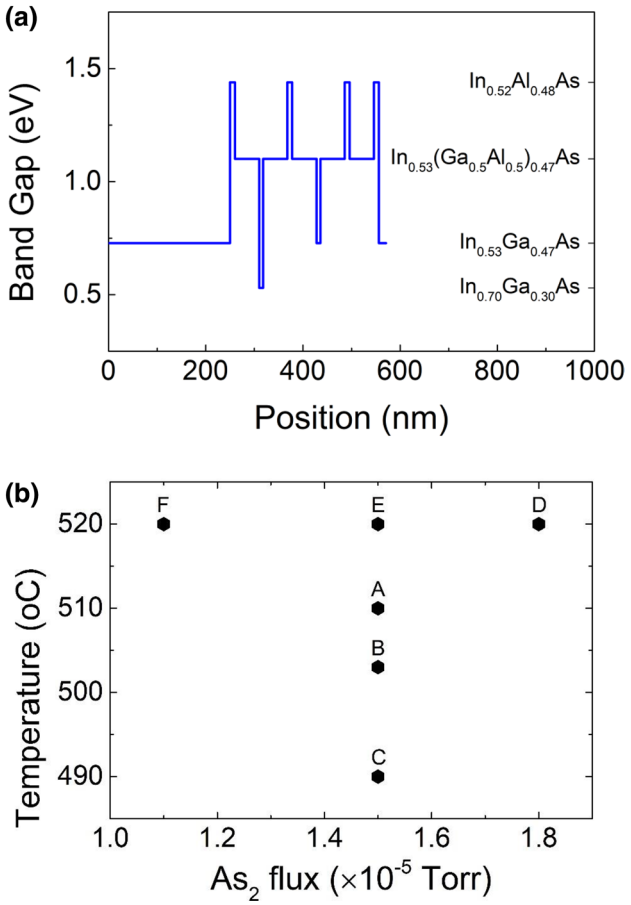

Fig. 4 **a** The test structure bandgap schema. The high bandgap InAlAs barriers were introduced to enable the simultaneous characterization of both the QWs and the InGaAlAs barriers. On the right axis the energies of band gaps are indicated for the materials of employed composition. **b** The growth conditions, substrate temperatures, and As_2 fluxes for the optimization of the heterostructure optical properties. The capital letters A–F enumerate the samples

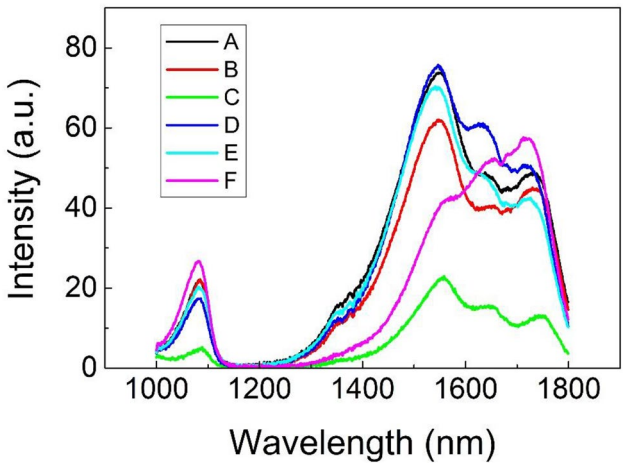

Fig. 5 The PL spectra taken for test samples grown under different growth conditions. The $In_{0.53}Ga_{0.47}As$ buffer layer and low and high indium content QWs require different growth conditions for maximum PL intensity. The lines described as A–F correspond to the PL spectra taken for the samples grown under the growth conditions marked in Fig. 4

for structures A, grown at 510 °C and 1.5×10^{-5} Torr of As_2, and D, grown at 520 °C and 1.8×10^{-5} Torr of As_2. These growth conditions are the same as those for the best optical quality $In_{0.53}Ga_{0.47}As$ buffer. The InGaAs emission was higher for higher substrate temperatures and higher As_2 fluxes. The $In_{0.53}(Ga_{0.5}Al_{0.5})_{0.48}As$ optical parameters are almost equal for all the samples, excluding the one grown at the lowest temperature of 490 °C.

For the epitaxy of the MECSEL structure, the growth conditions used for the F sample were applied (Fig. 5.), because this sample registered the highest efficiency of the PL emission from a highly strained QW. After growth, the MECSEL structure was tested with high resolution X-ray diffraction (HRXRD) and later in optical experiments. Since the MECSEL heterostructure consists of periodically spaced QWs and barriers, the X-ray diffraction data resembles those characteristics for superlattices (SLs). The thicknesses, the composition of the QWs and the barrier layers, and the strain of particular layers were obtained from the numerical analysis of the 2θ/ω curve using X'Pert Epitaxy and Smoothfit software. The experimental and simulated 2θ/ω data are shown in Fig. 6. The satellite peaks dominate the data due to diffraction on the 8 period SL consisting of the InGaAs QWs/InGaAlAs barriers. Other peaks that can be distinguished are caused by diffraction on the InP substrate, the InAlAs window, or the InGaAlAs barrier layers (Fig. 6a, b). The detailed analysis showed that even though the peaks due to diffraction on 8x(InGaAs/InGaAlAs) SL are narrow, they are split (Fig. 6c). The best fit of the simulated curve to the measured one was obtained assuming that the heterostructure consists of two different (InGaAs/InGaAlAs) SLs, and it was repeated four times. Consequently, it was determined that the composition of the QWs varied from the designed value by 2–3%. In contrast, the composition of the InGaAlAs barriers was very close to the expected value, $In_{0.52}(Ga_{0.5}Al_{0.5})_{0.48}As$. It is expected that such small composition deviations do not influence the optical properties of the laser. The results are summarized in Table 2.

The crystal quality and strain relaxation of the MECSEL structure was verified with reciprocal space mapping (RSM) independently in two directions, [110] and [−110]. The RSM measured in the [110] direction is presented in Fig. 7. For both directions, the reciprocal lattice points (RLPs) are narrow and diffuse scattering is not observed, which proves that the heterostructure is of high quality. The absence of the broadening of the RLPs along reciprocal space direction Q_x indicates that the structure is not bent. This observation was further confirmed by direct wafer curvature measurements; a radius equal to 40 m proves that the wafer is flat.

The RSMs have shown that the heterostructure is fully pseudomorphic; the stress due to layer mismatch is fully accumulated in the QWs and compensated in the barriers. Based on the HRXRD data, we calculated the strain

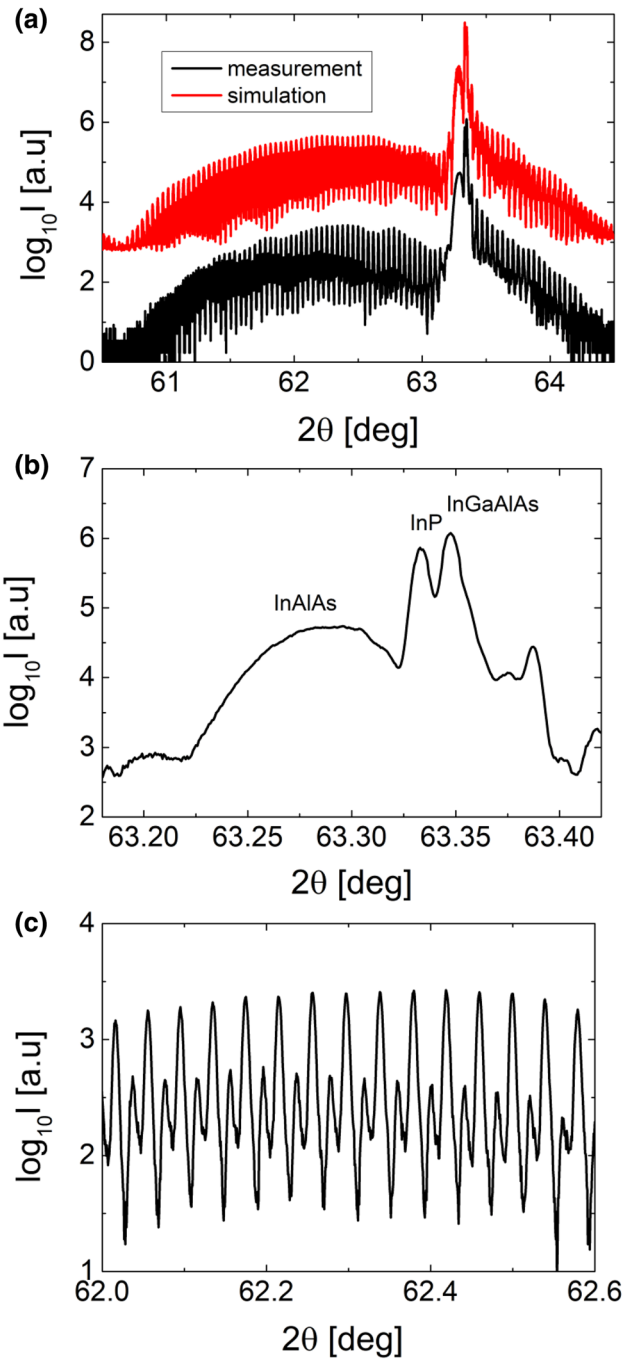

Fig. 6 **a** 004 high-resolution X-ray diffraction curve of the MECSEL structure (bottom, black line) compared with the simulated curve (upper, red line). **b** Detailed view of the diffraction peaks around the InP substrate. **c** Splitting of the diffraction peaks from the 8×(InGaAs/InGaAlAs) SL

distribution over particular layers and the average lattice mismatch of the QW/barrier SL. The identification of particular peaks in 2θ/ω to given layers is not straightforward when using HRXRD to investigate the multilayer structure, so the lattice constant calculations are based on the

Table 2 Thickness, composition and lattice mismatch of the QWs, InGaAlAs barriers and (InGaAs/InGaAlAs) SL

	Layer	No periods	Thickness [nm]	Composition			$\epsilon_{\perp}$ [ppm]	$\epsilon_{\parallel}$ [ppm]	$(\Delta a/a)_{\perp}$ (QW+barrier) [ppm]	$(\Delta a/a)_{\parallel}$ (QW+barrier) [ppm]
				In(x)	Ga(x)	Al(x)				
SL1	InGaAs QW	×4	8	0.67	0.33	–	9620	−9530	590	0
	InGaAlAs barrier		247.5	0.5259	0.237	0.2371	−2.8	2.8		
SL2	InGaAs QW	×4	8	0.68	0.32	–	10,330	−10,200	365	0
	InGaAlAs barrier		248.0	0.5239	0.238	0.2381	−139	140		

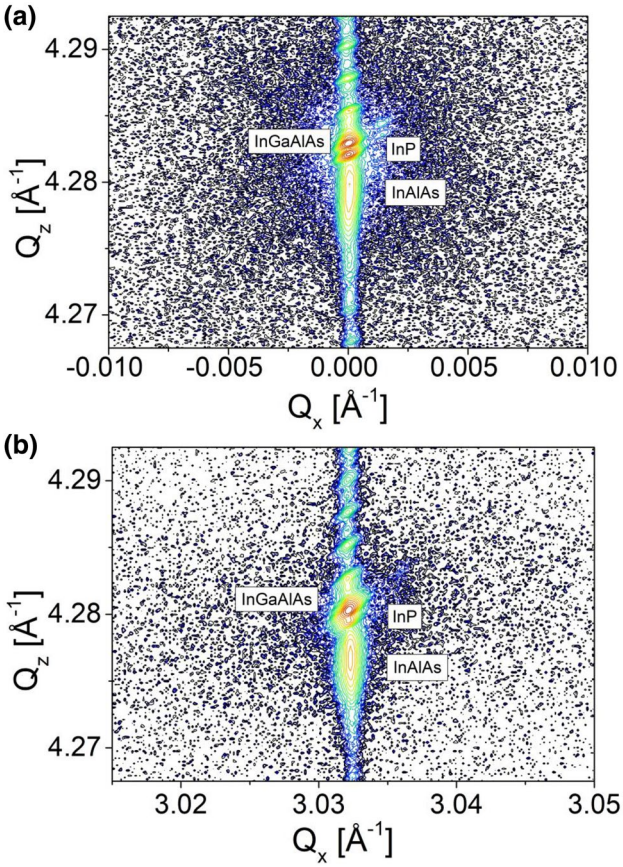

Fig. 7 Reciprocal space maps along the [110] direction for the MECSEL structure around a) the symmetrical 004 InP reciprocal lattice point and b) the asymmetrical (−2–24) InP reciprocal lattice point

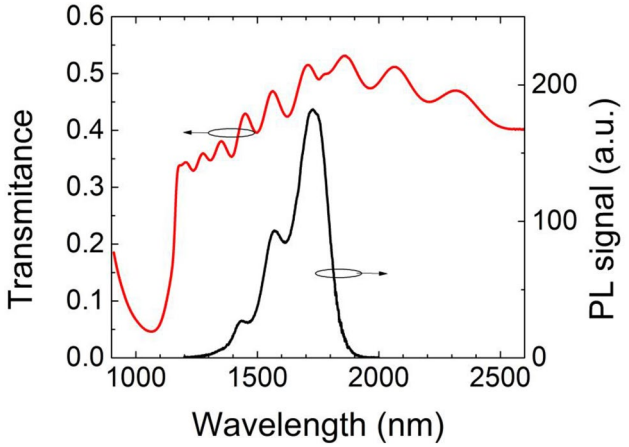

Fig. 8 Optical characterization of the MECSEL heterostructure. The transmission (left scale, red line) was measured after polishing the back side of the wafer. The PL data (right scale, black line) was taken from the wafer surface

parameters extracted from the simulated curve and Vegard's law.

The in-plane strain of the QWs was found to be nearly 1%, whereas the barrier layers remained unstressed. The calculated lattice mismatch for the QW/barrier SL was very low, approximately 360–570 ppm, which permitted pseudomorphic growth.

The PL spectra taken from the surface of the As-grown MECSEL wafer are shown in Fig. 8. The MECSEL signal is strongly modulated because of the RPG and Fabry–Perot modes. The main peak at 1727 nm and the peaks at 1564 nm and 1434 nm correspond to the 11, 12, and 13 Fabry–Perot etalon resonances, respectively.

The modulation of the optical properties by the etalon effect is especially visible in the optical transmission data. The transmission was measured after polishing the back side of the wafer. The Fabry–Perot (FP) modes are present starting from 1160 nm, which corresponds to the absorption edge of the $In_{0.5255}Ga_{0.2565}Al_{0.2245}As$ barrier layers. The modification of the FP mode at 1776 nm in the transmission spectra is due to two factors: the RPG resonance and the QW absorption. The drops in the amplitude of the oscillations in the transmission spectra towards short and long wavelengths are caused by absorption of QW and the free carrier absorption, respectively. The free carrier absorption is proportional to λ^2. The epitaxial heterostructure was deposited on n-doped substrates. The decrease of signal in the transmission was not present after substrate removal. The optical characterization showed that the QW emission is blue shifted with respect to the heterostructure's FP mode and coincident with a FP transmission valley. The origin of this discrepancy is

associated with limited precision of epitaxial growth and uncertainty of the reflection index of quaternary compounds.

After wafer characterization, the MECSEL heterostructure was subjected to post-growth processing. First, 2×2 mm^2 samples were separated from the wafer by cleaving. Then, the sample was capillary bonded to a transparent heat-spreader. Single $3\times3\times0.3$ mm^3 crystal diamonds were used. Next, the substrate was first mechanically thinned and then finally etched off completely. An HCl based solution was used since HCl dissolves the InP and does not etch the InGaAs etch-stop/surface protection layer. After etching, there was only a 2.85 µm-thick semiconductor membrane left on the diamond surface. In the next step, the membrane was covered with another diamond heat-spreader and they were slightly pressed against each other to stimulate the bonding. Finally, the chip consisting of diamond/membrane/diamond was set in a copper submount and set into the resonator (Fig. 3).

The excitation by collimated 980 nm pump radiation enabled the lasing. The pump spot was 225 µm in diameter. The MECSEL threshold was 2 W of absorbed power (Fig. 9a). The maximum power emission limited by thermal roll-over was 1.5 W at an absorbed pump power of 18 W. The ratio of the MECSEL thickness to the lateral diameter of the pump spot was 225/2.85 = ~80; the one-dimensional heat flow model can thus be applied for estimating the temperature increase along the growth axis of the heterostructure. The temperature distribution along the MECSEL heterostructure was calculated assuming uniform injection of carriers into the QWs and one-dimensional heat flow [31]. In the simulation, the heat-spreader's surface temperature was set to 2 °C and a pump power of 20 W was aimed at the spot 225 µm in diameter. The highest temperature was calculated to be 73 °C at the structure's centre. This temperature is not sufficient to stimulate the carriers' leakage from the QWs. Leakage alone does not explain the thermal roll-over of the power conversion characteristic (Fig. 9a); this can also be related to thermally activated Auger recombination. We sought to investigate further to clarify this issue. Our calculation shows that the highest temperature gradient is at the InAlAs window layers. The temperature increase along the window layers is equal to the temperature increase towards the centre of the heterostructure in four adjacent InGaAlAs barriers. Because the InAlAs layers exist to protect against the carrier escape towards the surfaces, they can be redesigned. Their thinning will enhance the heat extraction and lower the active region's temperature.

The laser operated in a multimode regime. The amplitude of the longitudinal modes was modulated by FP modes, due to the double diamond enclosing of the

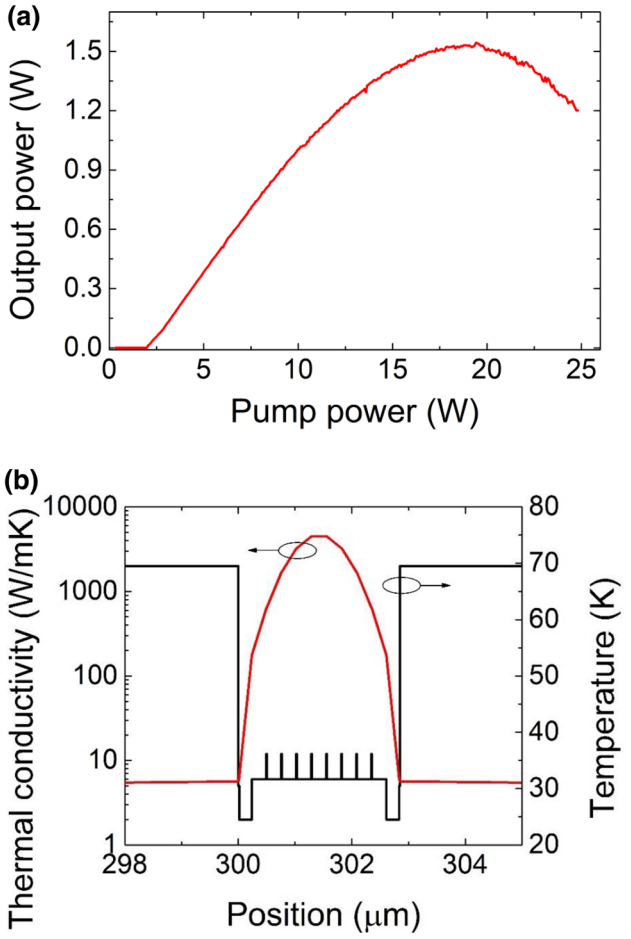

Fig. 9 **a** The power conversion characteristic of the MECSEL laser. **b** The thermal conductivity (left scale, black line) along the axes of symmetry for the MECSEL structure enclosed by two diamond transparent heat-spreaders. The temperature distribution (left scale red line), assuming uniform carrier injection into the QWs and one-dimensional heat flow

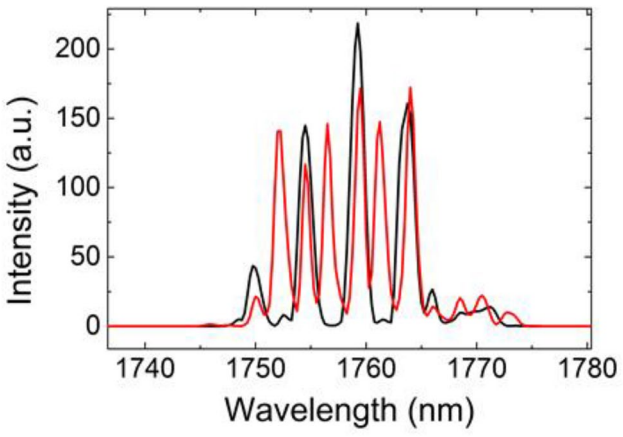

Fig. 10 The spectra registered at two positions on the diamonds/semiconductor membrane, in the centre of symmetric resonator (black line) and shifted out of the centre (red line)

MECSEL membrane (Fig. 10). Depending on the position of the heterostructure inside the resonator, each second FP mode could be switched off or on. This was due to the even symmetry of the heterostructure. When a heterostructure consists of eight equally separated QWs and is set centrally into a symmetric resonator, only the odd modes can be supported (see Fig. 2). The even modes have nodes at the QW positions, and thus are not gained. A small shift of the chip along the resonator axes, out of the central position, breaks the symmetry and consequently the even modes are also gained (Fig. 10). The spectra were centred at 1760 nm, in agreement with the PL data.

For the very first demonstration of the MECSEL, an unusually large redshift of the laser emission with respect to the spontaneous emission was reported [32, 33]. This redshift was attributed to bandgap shrinkage due to the high carrier concentration at and above the threshold [34]. Such redshift was not observed in our experiment, suggesting high quality of the epitaxial growth and post-growth processing.

4 Conclusion

We presented a high-power MECSEL emission in the 1750 nm band. The maximum power was 1.5 W at a holder temperature of 2 °C. In future work, the maximum power and efficiency can be further increased by a simple redesign of the window layers. The simple numerical model shows that the temperature increase in the active region of the MECSEL is relatively low, despite the 20 W of excitation. However, the influence of the temperature on the Auger recombination should be taken into account in further research.

The MECSEL in the 1750 nm spectral region is demonstrated for the first time. It was feasible to penetrate this spectra region with a surface-emitting high-power semiconductor laser because we did not use epitaxially grown DBRs. The only disadvantages are a slightly larger footprint and increased complexity of the optical resonator, where two external mirrors are used instead of one as in case of the more common VECSEL. The 1.5 W power makes the presented device applicable for Cr2+:ZnSe laser pumping. For this purpose, the simple and cost-efficient MECSEL can be an attractive alternative for more sophisticated lasers based on Tm-ions. The calibration of the growth parameters performed prior to growing the heterostructure showed that the optimum MBE growth parameters are different for QWs lattice-matched to InP than for strained QWs.

Acknowledgements The authors also wish to thank Krzysztof Czuba for his contributions in the measurements of transmission spectra.

Funding This work has been supported by the National Science Centre (NCN) in Poland through Grant No. 2017/25/B/ST7/00437.

References

1. Semiconductor disk lasers. Physics and technology. Edited by Oleg G. Okhotnikov, (2010) WILEY-VCH Verlag GmbH & Co. KGaA, Weinheim
2. A. Rahimi-Iman, J. Opt. **18**, 093003 (2016)
3. M. Guina, A. Rantamäki, A. Härkönen, J. Phys. D: Appl. Phys. **50**, 383011 (2017)
4. K.-S. Kim, J. Yoo, G. Kim, S. Lee, S. Cho, J. Kim, T. Kim, Y. Park, IEEE Photo. Technol. Lett. **19**, 1655 (2007)
5. E. Kantola, J.-P. Penttinen, S. Ranta, M. Guina, Electron. Lett. **54**, 1135 (2018)
6. T.-L. Heinen, M. Wang, A. Sparenberg, B. Weber, J. Kunert, S.W. Hader, J.V. Koch, M. Moloney, W. Koch, Stolz. Electron. Lett. **48**, 516 (2012)
7. A. Broda, I. Wójcik-Jedlińska, M. Sankowska, M. Wasiak, J. Więckowska, Muszalski. IEEE Photo. Technol. Lett. **29**, 2215 (2017)
8. A. Rudin, M. Rutz, D.J.H.C. Hoffmann, A.-R. Maas, E. Bellancourt, T. Gini, U. Südmeyer, Keller. Opt. Lett. **33**, 2719 (2008)
9. F. Zhang, B. Heinen, M. Wichmann, C. Möller, B. Kunert, A. Rahimi-Iman, W. Stolz, M. Koch, Opt. Express **22**, 12817 (2014)
10. A. Rantamäki, A. Chamorovskiy, J. Lyytikäinen, O. Okhotnikov, IEEE Photon. Technol. Lett. **24**, 1378 (2012)
11. A. Karim, J. Piprek, P. Abraham, D. Lofgreen, Y.-J. Chiu, J.E. Bowers, IEEE J. Sel. Top. Quantum Electron. **7**, 178 (2001)
12. V.-M. Korpijärvi, E.L. Kantola, T. Leinonen, R. Isoaho, M. Guina, IEEE J. Sel. Top. Quantum Electron. **21**, 1700705 (2015)
13. P. Holl, M. Rattunde, S. Adler, K. Scholle, S. Lamrini, P. Fuhrberg, E. Diwo-Emmer, R. Aidam, W. Bronner, J. Wagner, in Proceedings of SPIE 2017, pp 10087–1008705
14. L.A. Coldren, S.W. Corzine, M.L. Măsanović, *Diode Lasers and Photonic Integrated Circuits* (Wiley, New York, 2012)
15. S.W. Choi, K.S. Suh, J.W. Lee, J. Cryst. Growth **174**, 599 (1997)
16. S.T. Keller, A. Sirbu, V. Iakovlev, A. Caliman, A. Mereuta, E. Kapon, Opt. Express **23**, 17437 (2015)
17. J. Lyytikäinen, J. Rautiainen, A. Sirbu, V. Iakovlev, A. Laakso, S. Ranta, M. Tavast, E. Kapon, O.G. Okhotnikov, I.E.E.E. Photon, IEEE Photon Technol. Lett. **23**, 917 (2011)
18. J. Rautiainen, J. Lyytikäinen, A. Sirbu, A. Mereuta, A. Caliman, E. Kapon, O.G. Okhotnikov, Opt. Express **16**, 21881 (2008)
19. Z. Yang, A.R. Albrecht, J.G. Cederberg, M. Sheik-Bahae, Appl. Phys. Lett. **109**, 022101 (2016)
20. H. Kahle, C.M.N. Mateo, U. Brauch, P. Tatar-Mathes, R. Bek, M. Jetter, T. Graf, P. Michler, Optica **3**, 1506 (2016)
21. A. Jeżewski, I. Broda, A. Sankowska, K. Kumicz, K. Golaszewska-Malec, J. Czuba, Muszalski. Opt. Lett. **45**, 539 (2019)

22. Pics3D by Crosslicght, www.crosslight.com
23. L. Davis, Y.L. Lam, Y.C. Chen, J. Singh, P.K. Bhattacharya, IEEE J. Quantum Electron. **30**, 2560 (1994)
24. J.W. Matthews, A.E. Blakeslee, J. Cryst. Growth **27**, 118 (1974)
25. P. Blood, *Principles of Semiconductor Lasers in Semiconductor Lasers Fundamentals and Applications (Ed. Alexei Baranov and Eric Tournié)* (Woodhead Publishing Limited, Sawston, 2013)
26. S. Adachi, *Properties of Semiconductor Alloys: Group-IV, III–V and II–VI Semiconductors* (Wile, New York, 2009)
27. A. Broda, A. Kuźmicz, G. Rychlik, K. Chmielewski, A. Wójcik-Jedlińska, I. Sankowska, K. Gołaszewska-Malec, K. Michalak, J. Muszalski. Opti. Quantum Electron. **49**, 287 (2017)
28. S. Mirkhanov, A.H. Quarterman, H. Kahle, R. Bek, R. Pecoroni, C.J.C. Smyth, S. Vollmer, S. Swift, P. Michler, M. Jetter, K.G. Wilcox, Electron. Lett. **53**, 1537 (2017)
29. Z. Yang, D. Follman, A.R. Albrecht, P. Heu, N. Giannini, G.D. Cole, M. Sheik-Bahae, Electron. Lett. **54**, 430 (2018)
30. J. Muszalski, Thin Solid Films **367**, 299 (2000)
31. M. Szymański, Electron Technol. Internet J. **39**, 3 (2007)
32. Z. Yang, A.R. Albrecht, J.G. Cederberg, M. Sheik-Bahae, Opt. Express **23**, 33164 (2015)
33. H. Kahle, Ch. M. N. Mateo, U. Brauch, R. Bek, M. Jetter, Th. Graf, P. Michler. Vertical External Cavity Surface Emitting Lasers (VECSELs) VII, edited by Michael Jetter, in Proceedings of SPIE 2017, pp 10087–100870J
34. C. Wang, K. Malloy, M. Sheik-Bahae, Opt. Express **23**, 32548 (2015)